BIOCHEMISTRY
including biophysical chemistry & molecular biology

Article

pubs.acs.org/biochemistry

Solution Structure of Decorin-Binding Protein A from *Borrelia burgdorferi*

Xu Wang*

Department of Chemistry and Biochemistry, Arizona State University, Tempe, Arizona 85287, United States

Supporting Information

ABSTRACT: Decorin-binding protein A (DBPA) is an important lipoprotein from the bacterium *Borrelia burgdorferi*, the causative agent of Lyme disease. The absence of DBPA drastically reduces the pathogenic potential of the bacterium, and biochemical evidence indicates DBPA's interactions with the glycosaminoglycan (GAG) portion of decorin are crucial to its function. We have determined the solution structure of DBPA and studied DBPA's interactions with various forms of GAGs. DBPA is determined to be a helical bundle protein consisting of five helices held together by a strong hydrophobic core. The structure also possesses a basic patch formed by portions of two helices and two flexible linkers. Low-molecular mass heparin-induced chemical shift perturbations for residues in the region as well as increases in signal intensities of select residues in their presence confirm residues in the pocket are perturbed by heparin binding. Dermatan sulfate fragments, the dominant GAG type found on decorin, were shown to have lower affinity than heparin but are still capable of binding DBPA.

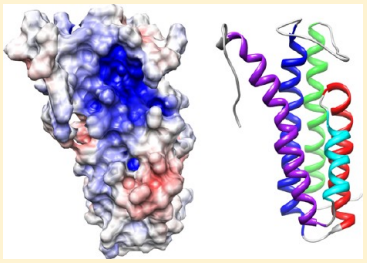

Lyme disease is a vector-borne illness spread by ticks infected with the bacterium *Borrelia burgdorferi*. Although the bacteria never enter the cell, their existence in the extracellular space can lead to local inflammations that produce symptoms from minor skin lesions to serious arthritis as well as heart and neural diseases if left untreated.[1] One important aspect of *Borrelia*'s existence as an extracellular bacterium is its extensive interactions with the extracelluar matrix. These interactions allow it to be extricated from blood and into surrounding tissues. In fact, the spread of *Borrelia* from blood to tissues is a prerequisite for chronic infection, which is resistant to antibiotic treatments that have proven to be effective in the treatment of early stage Lyme disease.[1−3] Development of a universal vaccine for the disease has proven to be difficult because of the wide genetic variability among different strains of *Borrelia*.[1,4] However, a few proteins have been identified as being crucial for *Borrelia* infectivity in humans and hold the potential for being useful therapeutic targets. One of the proteins is the lipoprotein decorin-binding protein (DBP). DBPs are membrane-anchored proteins expressed exclusively during the human host infection stage and were identified for being the primary adhesin for the small proteoglycan decorin,[5,6] an essential component in all collagen-based connective tissues whose absence greatly impairs the dissemination of *B. burgdorferi*.[7] Both variants of DBP (DBPA and DBPB) have been shown to be important to the *Borrelia* infection process, with the deletion of the genes encoding the proteins leading to defects in dissemination and early survival of the bacterium, presumably because of their inability to bind decorin and evade the immune system.[8−11]

Interactions of DBPs with decorin have already been characterized biochemically, and the protein is found to interact strongly with the glycosaminoglycan (GAG) part of decorin.[5,12,13] Leong and co-workers also investigated interactions of various strains of DBPA with GAGs using both in vitro and in vivo assays. Their studies demonstrated DBPA has affinity for both heparin and dermatan sulfate (DS), but not chondroitin sulfate (CS).[12−16] Interestingly, two studies also implicate the core protein of decorin in its interactions with DBPs.[5,14] To investigate the decorin-binding site on DBPA, sequence alignments and a peptide-based mutagenesis study have also been conducted. Several lysine residues on the protein have been shown to be crucial,[17,18] consistent with the conclusion that the glycosaminoglycan (GAG) portion of decorin is responsible for most of the interactions with DBPs. Similarly, an inadvertent mutation produced in the study conducted by Benoit et al. also showed the lysine-rich C-terminus of DBPA is also involved in binding GAGs.[14] Although the protein sequence of DBPB is relatively uniform among different strains of *Borrelia*, the DBPA sequence differs considerably from strain to strain. Biochemical studies conducted with transgenic strains of *Borrelia* showed different DBPA sequences have type-specific interactions with GAGs, raising the possibility that different strains of *Borrelia* may target different tissue types.[12]

Despite extensive biochemical and functional characterization, structural information about DBPs is scarce. It has been shown, by both secondary structure prediction and circular dichroism, that the protein is mostly α-helical. The secondary structure prediction also points to the existence of four helices in the protein, making the canonical four-helix bundle a likely conformation for DBPs. However, no high-resolution structure of the protein is available. This makes the interpretation of the available biochemical data difficult and

Received: May 30, 2012
Revised: September 17, 2012
Published: September 17, 2012

dx.doi.org/10.1021/bi3007093 | *Biochemistry* 2012, 51, 8353−8362

impedes our understanding of the mechanism by which DBPs achieve their GAG and decorin core protein recognition. In this paper, we present the solution structure of DBPA from *B. burgdorferi* strain B31 and nuclear magnetic resonance (NMR) characterization of its interactions with GAG fragments. DBPA is shown to be an all-helix protein. However, its conformation is an unusual helical bundle consisting of five helices. The helical bundle is held together by a strong hydrophobic core, while the surface of the protein is populated by both basic and acidic amino acids. Despite the presence of basic amino acids throughout DBPA, the electrostatic potential map of the protein reveals a well-defined basic pocket close to the C-terminus. In agreement with other biochemical studies, residues previously identified as being crucial to GAG−DBPA interactions in other strains of DBPA are found in the pocket. Low-molecular mass heparin-induced changes in chemical shifts and signal intensities of DBPA residues near the pocket provided proof that the basic patch most likely is involved in heparin binding. Interestingly, DS fragments did not induce chemical shift perturbations similar to those of heparin. Instead, the presence of DS hexasaccharide (dp6) produced severe signal broadening in DBPA. Besides NMR titrations, a gel mobility shift assay using fluorescently tagged GAG fragments was also conducted to characterize the GAG length dependence of DBPA−GAG interactions. The assay showed conclusively that DBPA binds heparin with a higher affinity than DS, and heparin fragments as short as a tetrasaccharide (dp4) can interact with the protein. Finally, after the N-terminal cysteine had been mutated to serine to prevent to dimerization, cystine chemical shift values confirmed that the two remaining cysteines at the C-terminal tail form an intramolecular disulfide bond.

EXPERIMENTAL PROCEDURES

Expression and Purification of DBPA. An open reading frame encoding the mature form of the B31 version of DBPA (residues 24−191) with the N-terminal cysteine mutated to serine was synthesized by Genscript Inc. (Piscataway, NJ) and cloned into the pHUE vector[19] as a chimera with His-tagged ubiquitin at the N-terminus. The plasmid was then transformed into BL21(DE3), and the transformed bacteria were grown to an OD_{600} of 0.8 at 37 °C before induction with 0.5 mM IPTG, followed by incubation for an additional 3 h at 30 °C. After the culture had been harvested, the resuspended cell pellet was lysed using sonication and fusion protein in the cleared supernatant was extracted through Ni-affinity chromatography using a 1 mL HisTrap column (GE Life Sciences). Specifically, cleared supernatant in 20 mM sodium phosphate buffer (pH 8.0), 10 mM imidazole, and 500 mM NaCl was loaded onto the column at a flow rate of 1 mL/min. The column was washed with 35 mM imidazole for 5 min before an imidazole gradient of 35 to 500 mM was applied to elute the protein. After the buffer had been exchanged with 25 mM Tris (pH 8.0) and 100 mM NaCl, the purified fusion protein was digested with ubiquitinase USP2 overnight at room temperature.[19] The cleaved DBPA was separated from His-ubiquitin and His-tagged ubiquitinase by passing the mixture through a Ni-affinity column and collecting the flow-through. Unlabeled protein was obtained by growing the culture in normal LB, and isotopically labeled DBPAs were obtained by expressing the protein in M9 medium supplemented with $^{15}NH_4Cl$ or [^{13}C]glucose.

Analytical Size Exclusion Chromatography of DBPA. To characterize the oligomerization state of DBPA, DBPA was subjected to analytical size exclusion chromatography using a 160 mL Superdex 75 gel filtration column (GE Lifesciences). The column was first equilibrated in 50 mM sodium phosphate (pH 6.5) and 300 mM NaCl; 100 μL of 0.6 mM DBPA was then injected onto the column, and the flow rate was held at 0.7 mL/min for a total elution volume of 130 mL. The elution time of DBPA was compared to standards with known molecular masses (Bio-Rad, catalog no. 151-1901).

Glutaraldehyde Cross-Linking Assay. A solution (100 μL) containing either 5, 12.5, 25, or 50 μM DBPA in 20 mM HEPES buffer (pH 7.5) was cross-linked by the addition of 5 μL of 2.5% glutaraldehyde and incubation at 37 °C for 5 min. The reaction was quenched with 10 μL of 1 M Tris (pH 8.0), and 5 μg of protein from each reaction mixture was analyzed by SDS−PAGE.

Acquisition and Analysis of NMR Data for DBPA Structure. NMR data on DBPA were collected on an Agilent Inova 800 MHz spectrometer equipped with a cryogenically cooled triple-resonance probe and a Varian Inova 500 MHz spectrometer with a room-temperature probe. Most pulse sequences were based on experiments included in the pulse sequence package BioPack (Agilent Inc.). For backbone assignment, HNCACB, HNCO, HNCOCA, HNCOCACB, and HNCOCA spectra of ^{2}H-, ^{13}C-, and ^{15}N-labeled DBPA were collected. ^{15}N- and ^{13}C-edited NOESY-HSQC spectra of ^{13}C- and ^{15}N-labeled DBPA were collected for the determination of structure. Assignments of methyl groups were made using the methyl HCCH-TOCSY experiments, and assignments of other side chain protons were made using ^{13}C-edited NOESY-HSQC. HN and NC residual dipolar couplings (RDCs) of DBPA aligned in a 7% neutral polyacrylamide gel were collected on ^{2}H-, ^{13}C-, and ^{15}N-labeled DBPA using J-modulated pulse sequences from Liu et al.[20] Residue-specific rotational correlation times were calculated using the procedure outlined by Liu et al.[21] Samples used in data collection contain 0.6−1 mM DBPA and 50 mM sodium phosphate (pH 6.5). To confirm the absence of intermolecular NOEs, the two-dimensional ^{13}C- and ^{15}N-filtered, ^{13}C-edited NOESY spectrum of DBPA was collected on a 1 mM DBPA sample containing 0.5 mM ^{13}C- and ^{15}N-labeled DBPA and 0.5 mM unlabeled DBPA. The pulse sequence used was the gCNfilnoesyChsqcA sequence from Biopack, and 256 transients accumulated for each FID. All data processing was done with NMRPipe[22] and analyzed in NMRView.[23]

Structure Determination. Backbone dihedral angles of well-ordered residues were calculated with TALOS.[24] Isotopically edited NOESY-HSQC data for DBPA were first analyzed and assigned manually with the focus on finding unambiguous long-range contacts. The partially assigned NOESY-HSQC peak lists were then used in CYANA's default automatic structure determination protocol.[25] The resulting structure and final constraint table were used in XPLOR-NIH for final refinement with RDCs.[26] The 10 structures with the fewest NOE violations were used in the ensemble presented here.

Production of Low-Molecular Mass GAG Fragments. Heparin and DS were purchased from Sigma Aldrich. All GAGs were dialyzed and lyophilized to remove excess salt. Short GAG fragments were obtained through enzymatic partial depolymerization. Porcine mucosa heparin was depolymerized with heparinase I (IBEX Inc.) until the digestion was 30% complete.[27] Porcine mucosa DS fragments were also obtained through 30% partial digestion by Chondroitinase ABC (Sigma Aldrich).[28] In both cases, the fragments were separated on the

dx.doi.org/10.1021/bi3007093 | *Biochemistry* 2012, 51, 8353−8362

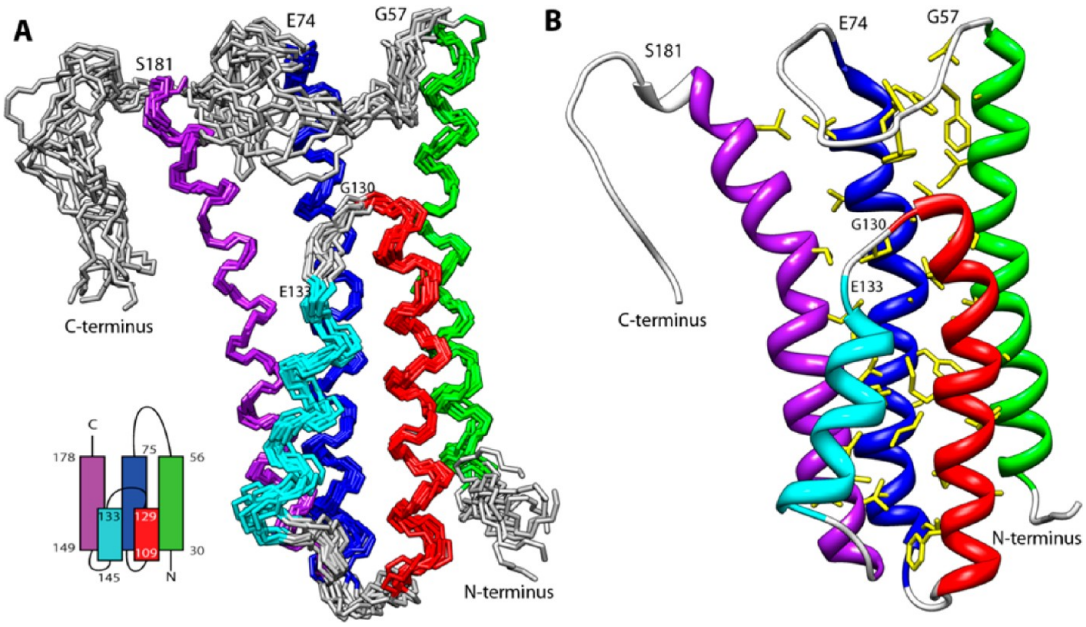

Figure 1. (A) Ensemble of the 10 lowest-energy structures of DBPA in solution. Helix 1 (residues 30−56) is colored green. Helix 2 (residues 75−104) is colored blue. Helix 3 (residues 109−129) is colored red. Helix 4 (residues 133−145) is colored cyan. Helix 5 (residues 149−178) is colored purple. The schematic topology of the protein is shown at the bottom left. (B) Ribbon depiction of DBPA with the side chains of amino acids in the hydrophobic core colored yellow.

basis of size using a 2.5 cm × 175 cm size exclusion chromatography column (Bio-Rad Biogel P10) and a flow rate of 0.2 mL/min. Fractions containing the same size fragments were pooled, desalted, and lyophilized. The sizes of the DS fragments were verified with ESI-MS, and the sizes of heparin fragments were inferred using DS as a standard. The amount of GAG fragments was determined gravimetrically after lyophilization. The longest DS fragment isolated is dp14, and the longest heparin fragment isolated is dp10. The disaccharide compositions of the GAGs were analyzed by exhaustively digesting the GAGs using the appropriate lyases and separating the resulting disaccharides by SAX−HPLC. The identities of the disaccharides were determined by comparing their elution times to standards with known structure.

Gel Mobility Shift Assays for DBPA. Gel mobility shift assays were conducted using the method of Seo et al.[29] Briefly, DS and heparin fragments (dp4, dp6, dp8, and dp10) were fluorescently labeled with 2-aminoacridone using the method of Lyon et al.[30] Two micrograms of the fluorescently labeled GAG was then mixed with either 1 molar equiv of DBPA in 50 mM sodium phosphate buffer (pH 6.5) and 150 mM NaCl buffer or an equal volume of the same buffer without the protein and incubated for 30 min. The mixtures were subjected to electrophoresis at 120 V for 20 min in a 1% agarose gel with 40 mM Tris, 20 mM acetate, 1 mM EDTA buffer (pH 8.0). The positions of the fragments were visualized using a UV panel.

Titrations of DBPA with Heparin and DS. Titrations of DBPA with the intact GAG polymer were conducted by adding 200 μg of intact polymer to a 400 μL sample containing 200 μM DBPA in 50 μg aliquots. For titrations of DBPA with heparin dp6, heparin dp10, and DS dp14, aliquots of a 40 mM polysaccharide stock solution were added to 400 μL of 100 μM DBPA in 50 mM sodium phosphate (pH 6.5) and 150 mM NaCl at concentrations of 0.3, 0.6, 0.9 1.2, 1.6, and 2.0 mM. For the titration of DBPA with DS dp6, aliquots of a 40 mM DS dp6 stock solution were added to 400 μL of 200 μM DBPA at concentrations of 0.4, 1.0, and 1.6 mM. A $^{1}H-^{15}N$ HSQC spectrum was acquired at each point to monitor the titrations. Chemical shift changes in both ^{1}H and ^{15}N dimensions were combined into a single normalized chemical shift value according to ref 31. Specifically, normalized chemical shift δ_n is defined by the equation $\delta_n = [\Delta\delta_H^2 + (1.7 \times \Delta\delta_N)^2](1/2)$, where $\Delta\delta_H$ and $\Delta\delta_N$ represent chemical shift changes in hertz for the ^{1}H and ^{15}N dimensions, respectively. The K_d of binding was extracted by fitting plots of normalized chemical shift changes relative to ligand concentration using the 1:1 binding chemical shift fitting feature in xcrvfit (http://www.bionmr.ualberta.ca/bds/software/xcrvfit/). The DS dp6 concentration-dependent signal decay rate was extracted by measuring HSQC peak intensities at different DS dp6 concentrations and fitting the plot of intensity versus DS dp6 concentration to the equation $I([DS]) = I(0)e^{-[DS]R}$, where [DS] is the concentration of DS dp6, I is the intensity of the signal, and R is the rate constant governing the decay. Data for the titrations were acquired on a Varian 800 MHz Inova spectrometer.

RESULTS

Oligomerization State of DBPA. Native DBPA containing the N-terminal cysteine was known to form dimers.[5,18] To prevent the dimerization of DBPA in this study, we mutated the N-terminal cysteine to serine. However, the broadness of DBPA's NMR signals is typical of a larger protein. To test whether DBPA oligomers exist, DBPA was subjected to glutaraldehyde cross-linking at pH 7.5. Significant dimer formation was detected at concentrations of >10 μM (Figure S1A of the Supporting Information). Species corresponding to trimers were also seen at higher concentrations, indicating the protein can aggregate nonspecifically at high concentrations. Because the cross-linking reaction is nonreversible, the results are only a qualitative indication that oligomers exist. More accurate characterization of oligomer fractions was conducted

dx.doi.org/10.1021/bi3007093 | Biochemistry 2012, 51, 8353−8362

using size exclusion chromatography and NMR rotational correlation times. When DBPA was analyzed using size exclusion chromatography, the protein eluted slightly earlier than the 17 kDa molecular mass standard and modest aggregation was seen (Figure S1B of the Supporting Information). Thus, size exclusion chromatography indicates the oligomerization equilibrium is heavily biased toward the formation of monomers. The rotational correlation times of the protein were determined to be around 15 ns for structured regions of DBPA (Figure S2 of the Supporting Information). Compared with correlation times of proteins with known apparent molecular masses, this corresponds to a mass of 25 kDa. Because the monomer molecular mass is only 19 kDa, the larger apparent mass indicates roughly 30% of protein exists in dimer form under NMR conditions. These data corroborate the theory that although oligomers are present, they are the minor fraction. Because intermolecular NOEs misinterpreted as intramolecular NOEs are known to produce incorrect NMR structures,[32] a $^{13}C/^{15}N$-filtered, ^{13}C-edited NOESY-HSQC experiment was performed on a 1 mM DBPA sample containing half ^{13}C- and ^{15}N-labeled DBPA and half unlabeled DBPA. No credible intermolecular NOE cross-peaks were detected (Figure S3 of the Supporting Information). Some weak peaks corresponding to NOE contacts between ^{1}H with chemical shifts of 4.1 and 1.9 ppm were seen. However, these are most likely residual signals from strong intraresidue contacts between Hα and Hβ atoms. No cross-peaks were seen in crucial regions where hydrophobic core protons are found, eliminating the possibility that the hydrophobic core structure, which largely determines the three-dimensional fold of the protein, is distorted because of intermolecular NOE contamination. The signal broadening observed in the NMR data is most likely caused by exchanges between oligomer and monomer. Because the density of DBPA on bacterial membrane is not known, it is unclear whether the aggregation occurs in vivo.

Structure of DBPA. The mature form of DBPA (residues 24−191) was predicted to consist of four α-helices. Although the experimental data were consistent with DBPA being mostly helical, an unstructured region was found in one of the predicted helices (residues G130−E133), leading to five helices in the protein instead of four. Further examination of the NOE contact pattern between the helices showed the two halves of the predicted third helix are antiparallel to one another. Figure 1A shows the ensemble of structures most consistent with the experimental data. Table 1 contains the structural statistics for the ensemble. Overall, DBPA adopts a five-helix bundle conformation. The partition of the predicted helix three into two antiparallel helices altered the topology of the protein such that the long linker between helices 1 and 2 is proximate to the C-terminal tail. The helical bundle is held in place by a tightly packed hydrophobic core involving 31 residues (Figure 1B). Helices 1−3 are perfectly parallel to each other, while helices 4 and 5 are at an angle with the other helices. Helix 2 is central to the formation of the hydrophobic core, with 11 residues in the helix making hydrophobic contacts with residues in helices 1, 3, and 5. Helices 3 and 5 also form parts of the core by making contacts with each other as well as helix 2. The short helix 4 sits at the periphery of the core, making minor contacts with helices 3 and 5 only. The angled orientation of helix 4 and part of helix 5 are reflected in the values of their backbone HN residual dipolar couplings: RDCs for consecutive residues in both helices 4 and 5 experience large cyclic oscillations in their values, an indication that parts of helices are not perfectly parallel to a single dominant alignment axis (Figure S4 of the Supporting Information). Despite its small size and weak contacts with the core, rotational correlation time measurement shows helix 4 is as rigid as the rest of the protein (Figure S2 of the Supporting Information), confirming that its position relative to the rest of the protein is stable. However, helix 4 in the structure ensemble shows a backbone root-mean-square deviation (rmsd) of 0.85 Å, larger than the rmsd of 0.60 Å for residues in other helices. This coupled with the observation of smaller RDCs for residues in helix 4 and the fact that RDC values are very sensitive to the presence of motional averaging shows helix 4 may undergo more internal motion than other helices. A structural homology search using the Dali server[33] found no significant homology between the DBPA structure and those already in the Protein Data Bank.

Besides the helical regions, the protein also contains two large disordered segments: the flexible linker between helices 1 and 2 (residues G57−E74) as well as a long C-terminal tail.

Table 1. Structural Statistics for the Ensemble of DBPA Structures

no. of NOE-based distance constraints	
total	1171
intraresidue ($i = j$)	81
sequential ($\|i - j\| = 1$)	242
medium-range ($1 < \|i - j\| < 5$)	396
long-range ($\|i - j\| \geq 5$)	452
NOE constraints per restrained residue[a]	7.3
no. of residual dipolar couplings	
H−N	113
N−C	103
no. of dihedral angle constraints	210
total no. of structures computed	100
no. of structures used	10
residual constraint violations[b]	
no. of distance violations per structure	
0.1−0.2 Å	15
0.2−0.5 Å	8
>0.5 Å	0
no. of dihedral angle violations per structure	
1−10°	11
>10°	0
no. of RDC violations per structure	
0−1 Hz	3
>1 Hz	0
rmsd	
all backbone atoms	1.4 Å (all), 0.6 Å (ordered[c])
all heavy atoms	1.9 Å (all), 1.1 Å (ordered[c])
Ramachandran plot summary from Procheck[d] (%)	
most favored regions	98.0
additionally allowed regions	1.8
generously allowed regions	0.2
disallowed regions	0.0

[a]There are 160 residues with conformationally restricting constraints. [b]Calculated for all constraints for the given residues, using a sum over r^{-6}. [c]Residues with a sum of ϕ and ψ order parameters of >1.8. Ordered residue ranges of 31−55, 76−103, 110−128, 134−142, and 145−179. [d]Residues selected on the basis of dihedral angle order parameter, with $S(\phi) + S(\psi) \geq 1.8$. Selected residue ranges of 31−55, 76−103, 110−128, 134−142, and 145−179.

dx.doi.org/10.1021/bi3007093 | Biochemistry 2012, 51, 8353−8362

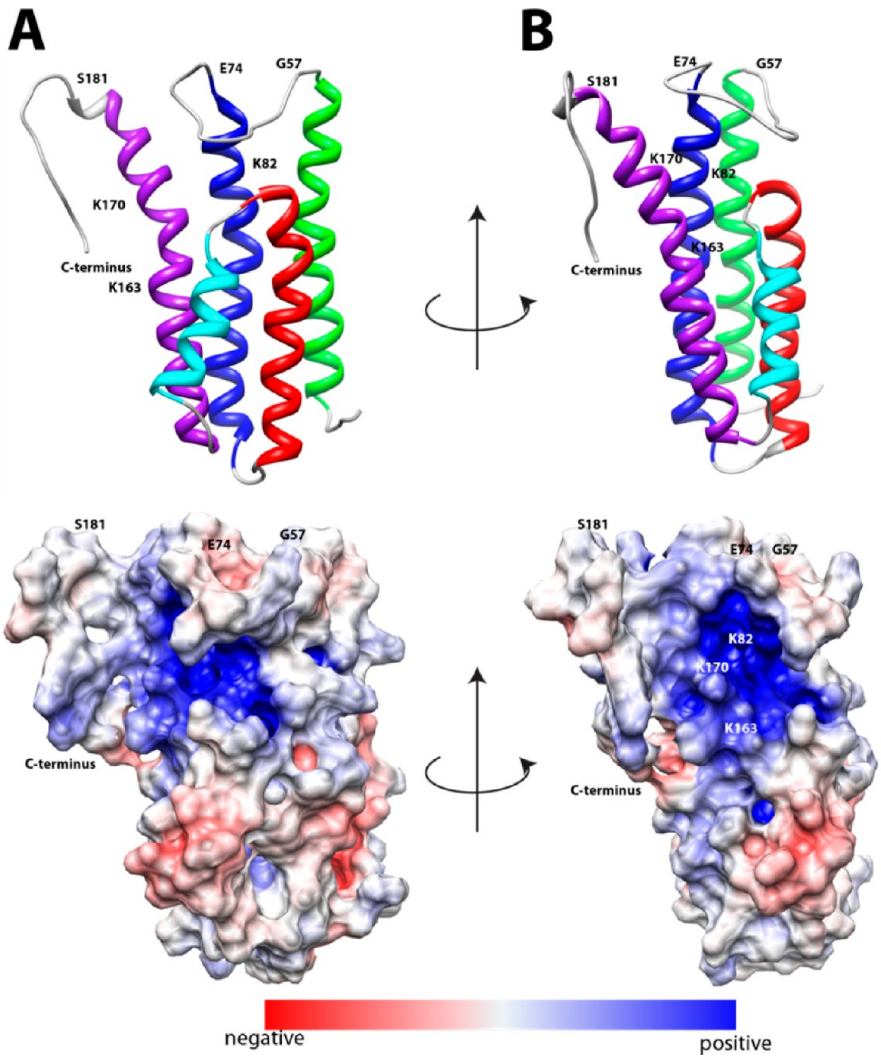

Figure 2. Electrostatic potential surface map of DBPA in two orientations. Red indicates acidic regions and blue basic regions. (A) Protein in the same orientation as in Figure 1A. (B) Protein rotated 90° about the vertical axis.

Residues in both regions possessed lower rotational correlation times typical of flexible, dynamic segments (Figure S2 of the Supporting Information). The C-terminal tail contains the only two cysteines in the protein. Cβ chemical shifts of the cysteines in the absence of reducing agents indicate they are involved in the formation of disulfide bonds. To determine whether the disulfide bond is inter- or intramolecular, SDS−PAGE was performed under nonreducing conditions and no dimers were seen. HSQC spectra of the protein under reducing conditions (10 mM DTT) were also collected: although many C-terminal residues did experience a decrease in rotational correlation time, corresponding to an increase in dynamics, the overall correlation time for the protein did not change. These observations confirm that the disulfide bond formed is intramolecular. Because the C-terminal tail is a potential GAG-binding segment in the protein, GAG binding affinities of reduced and oxidized DBPA were tested: no significant difference was detected. However, the reduced C-terminal tail of the protein did show more signs of degradation than the oxidized version.

DBPA possesses a large number of basic residues typical of GAG-binding proteins. They are spread throughout the protein, but a particularly high concentration can be found on the last helix. The protein also contains a significant number of acidic residues, which are interspersed among the basic residues, leading to a neutralization of the charges in some areas. Figure 2 is the electrostatic potential map of the protein. A large basic patch composed of the second half of helices 2 and 5, the C-terminal tail, and the linker between helices 1 and 2 can be seen. Despite basic residues in other regions of the protein, they appear to have neutral to weakly acidic potential. In agreement with previous studies, residues known to be important in DBPA−GAG interactions, which include lysines 82, 163, and 170 and the C-terminal tail,[14,17,18] are found in the basic patch (Figure 2).

Interactions of DBPA with GAGs. To gain further insight into DBPA's GAG binding mechanism and to confirm the role of the basic pocket in binding GAGs, DBPA's interactions with DS and heparin, the two types of GAGs known to bind DBPA, were examined. Addition of heterogeneous polysaccharides of both species of GAGs weakened the NMR signals of DBPA greatly and without discrimination, but none were able to produce observable changes in DBPA chemical shifts. This phenomenon is often seen in GAG-binding proteins, and the most plausible interpretation of the results is that interaction of DBPA with the long GAG chains led to extreme signal

dx.doi.org/10.1021/bi3007093 | *Biochemistry* 2012, 51, 8353−8362

broadening of GAG-bound proteins because of the large size of the complex produced through a combination of GAG-induced oligomerization and multiple-ligand binding; thus, only free DBPA contributes to detectable NMR signals. This shows DBPA indeed interacts with heparin and DS but provides no information about the GAG-binding epitope of DBPA. To study the GAG-binding epitope on DBPA, we examined DBPA's interactions with low-molecular mass GAGs. The use of short fragments not only reduces the molecular mass of the polysaccharides but also diminishes the level of GAG-induced oligomerization of protein. However, because multivalency of GAGs is a crucial factor in protein−GAG interactions, short fragments of GAG are expected to have a lower binding affinity than native polysaccharides. For this study, the dependence of the GAG−DBPA interaction on GAG length is investigated using gel mobility shift assays, and DBPA was also titrated with heparin dp6 and dp10 as well as DS dp6 and dp14. Although the sulfation patterns of the fragments used are heterogeneous, disaccharide analyses of the GAGs can provide some insights into the sulfation density of the fragments. Disaccharide analysis showed heparin contains 70% trisulfated disaccharide units with the rest being mostly disulfated disaccharides. The DS fragments analyzed via SAX−HPLC showed more than 90% of disaccharides from DS are monosulfated, confirming previously published analysis of DS from the same source.[28] In agreement with the law of probability, 30% of dp6 fragments contain at least one disulfated unit and 50% of dp14 fragments contain at least one disulfated unit. These distributions show the DS used is sufficiently uniform that chondroitinase ABC cleavage sites are not significantly biased by sulfation patterns.

A qualitative characterization of DBPA−GAG interactions was conducted using the gel mobility shift assay and fluorescently labeled GAG fragments according to Seo et al.[29] (Figure 3). Migrations of all heparin fragments were affected

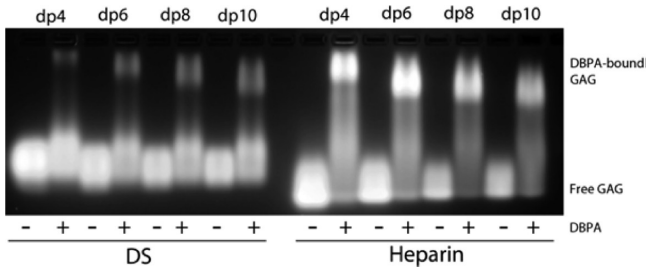

Figure 3. Gel mobility shift assay of heparin and DS fragments in the presence and absence of DBPA. The mobility of fluorescently tagged GAG fragments is greatly retarded by their binding to DBPA.

significantly by the presence of DBPA. However, only a small percentage of DS fragments were shifted by DBPA, even at a length of dp10. These observations agreed with previous studies conducted using native GAG polymers, which showed heparin is a more potent inhibitor of bacterial adhesion than DS.[15,34]

To quantitatively measure the interaction affinity and to map out the GAG binding epitope on DBPA, the protein was titrated with several GAG fragments of fixed length and monitored using NMR. Figure 4 is the overlay of $^{1}H-^{15}N$ HSQC spectra acquired at each titration point of DBPA−heparin dp10 titration. Interactions of DBPA with heparin dp10 fall in the fast exchange time scale, and small but significant chemical shift changes can be seen in several residues. Figure

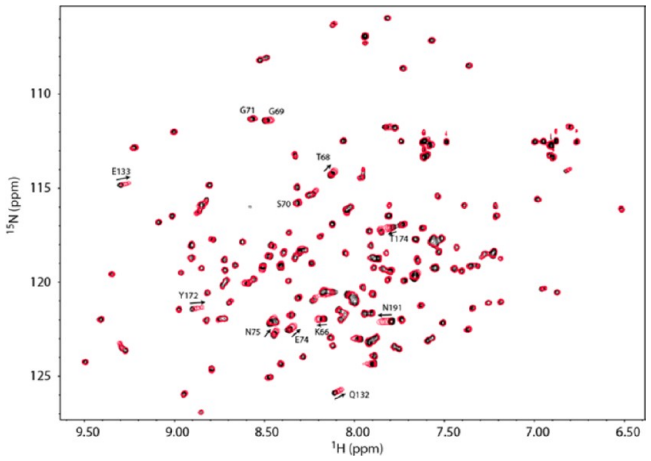

Figure 4. $^{1}H-^{15}N$ HSQC overlays of DBPA in the presence of different concentrations of heparin dp10. Signals experiencing a large migration or a large increase in signal intensity (G69, S70, and G71) are indicated with the residue number and direction of migration. The solid black contour represents the starting HSQC spectrum of DBPA in the absence of heparin dp10. Each subsequent red single contour represents the HSQC spectrum of DBPA at a different concentration of heparin dp10. The concentrations of heparin dp10 are 0.3, 0.6, 0.9, 1.2, 1.6, and 2.0 mM. The DBPA concentration is 0.1 mM.

5A shows residue-specific perturbations to $^{1}H-^{15}N$ chemical shifts by heparin dp10, and Figure 5B shows the same information mapped onto the surface of DBPA. The most perturbed residues include K64, D65, K67, T68, S73, E74, N75, V122, Q132, E133, H168−K170, and N191. Many of the residues reside in the flexible region from residue G57 to E74. Most of the residues are located at or near the basic patch in the electrostatic potential surface map, identifying the basic patch as the most likely heparin binding epitope of DBPA. One especially notable change not illustrated by the chemical shift mapping was that residues G69−G71 in the flexible linker showed significant increases in signal intensity. Magnitudes of signals corresponding to G71 and G69 increased 30%, while that of S70 increased 50%. This is in contrast to the loss of signal intensity of 10−50% experienced by other residues. The most plausible explanation for the observation is that heparin binding in the vicinity of these residues has prevented the labile amide protons from exchanging with solvents as exchanges between solvent protons and amide protons attenuate signal intensity, or the binding of heparin shifted the dynamic time scale of the flexible linker into a regime that no longer induces signal broadening. This occurrence shows the flexible linker may play a significant role in heparin binding. Examination of the flexible linker sequence showed it contains a BXBB motif (K64, D65, K66, and K67), which is often associated with GAG binding. The existence of such a motif therefore further enhances the role of the linker in GAG interactions. Titration of DBPA with heparin dp6 produced similar chemical shift migration changes (Figure S5A of the Supporting Information), and using the chemical shift changes of N191 and Q132, which are among the most significant in the protein, the K_d of binding for dp10 was calculated to be in the range of 1−4 mM (Figure S5B of the Supporting Information). Surprisingly, the K_d of binding for the shorter dp6 fragment is comparable (Figure S5B of the Supporting Information).

Limited amounts of DS dp6 and dp14 were also obtained by partial depolymerization of DS using chondroitinase ABC. DS

dx.doi.org/10.1021/bi3007093 | *Biochemistry* 2012, 51, 8353−8362

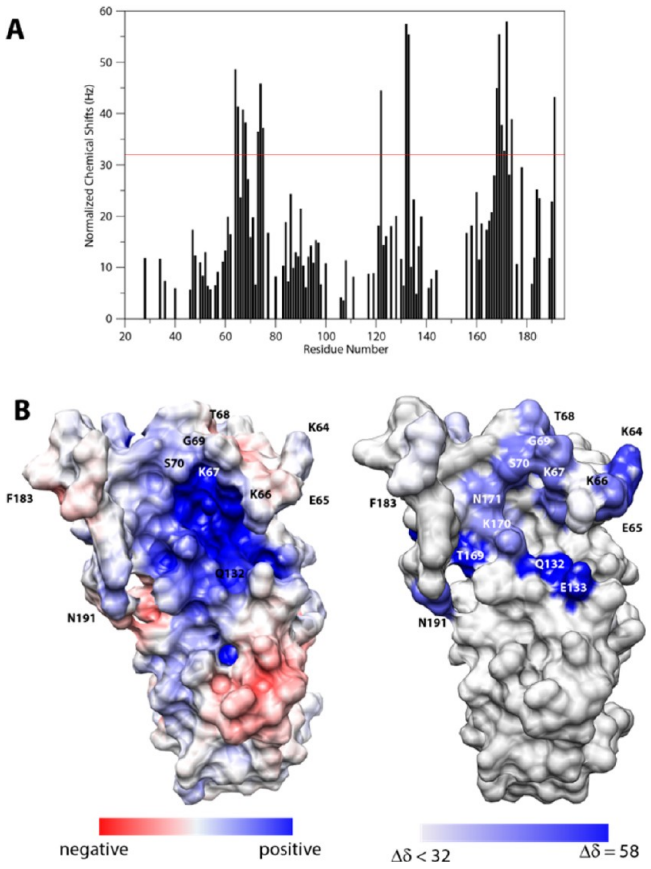

Figure 5. (A) Normalized chemical shift perturbations to backbone amide nitrogen and proton by heparin dp10. The red line represents the value of perturbation 1.5 standard deviations higher than the average. (B) Comparison of the electrostatic potential map of DBPA (left) and heparin perturbation map of DBPA. The DBPA perturbation map is colored according to the chemical shift perturbation values shown in panel A. The most perturbed residues are colored deep blue.

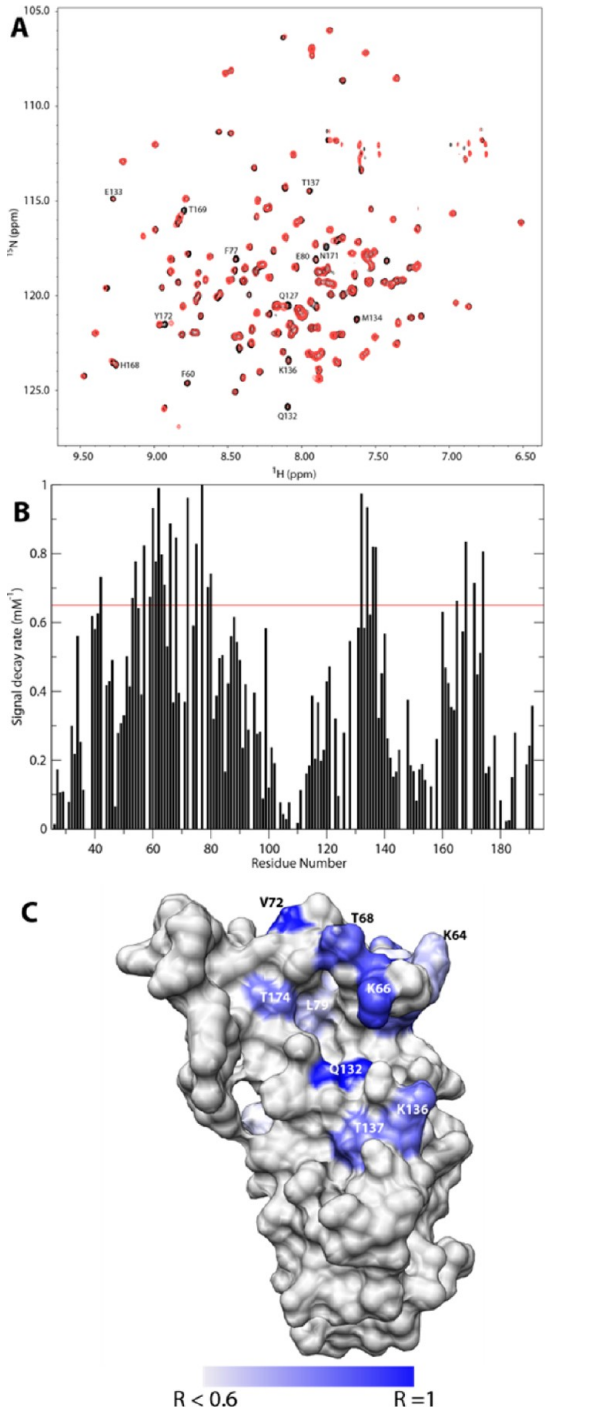

Figure 6. (A) Superimpositions of HSQCs of 0.2 mM DBPA with no DS dp6 (black) and with 1.2 mM DS dp6 (red). (B) Plot of the residue-specific signal decay rate. (C) Locations of residues experiencing severe DS-induced signal decay. Residues having a decay rate of ≥0.6 mM^{-1} are colored in increasingly deeper shades of blue. *R* stands for the decay rate. DBPA is in the same orientation as in Figure 2B.

dp6 induced very little chemical shift change when added to DBPA (Figure 6A); even at a protein:GAG ratio of 1:8, the increases in the peak intensity of residues G69−G71 seen in the heparin titration were not observed either. Only residues Q127, T169, and Y172 demonstrated detectable chemical shift changes. However, large decreases in peak intensities were observed for a selective set of residues during the titration. Through a yet-not-well-understood mechanism, the decreases in peak intensities appear to form a single-exponential decay curve when plotted versus DS dp6 concentration (Figure S6 of the Supporting Information). This allowed the GAG-induced rate of signal decrease to be extracted for each residue in the protein by fitting the curve using the equation $I([DS]) = I(0)e^{-[DS]R}$, where [DS] is the concentration of DS dp6, *I* is the intensity of the signal, and *R* is the rate constant governing the decay. Figure 6B shows the plot of *R*, rate of signal decrease, versus residue number, and Figure 6C shows the same information visualized on the surface representation of DBPA. The profile is very similar to the plot of heparin-induced chemical shift perturbation. Residues that experienced large decreases in intensity include F60, A62, K66, V72, F77, Q132, M134, K136, T137, H168, and T174, almost all of which can be located around the basic pocket, with a very high concentration found in the flexible linker and helix 5. Of the three residues that experienced large GAG-induced signal intensity boosts, G69 and G71 showed a modest decline in signal intensity while S70's signal intensity remained almost constant. The trend followed by these three residues is contrary to those surrounding them in the flexible linker, most of whom experienced large signal decreases. Because of the lack of observed chemical shift changes in the titration, no dissociation

dx.doi.org/10.1021/bi3007093 | *Biochemistry* 2012, 51, 8353−8362

constant of binding can be extracted. Titration of DBPA with DS dp14 also led to signal decreases similar to those seen in the DS dp6 titration. Not surprisingly, the rate and extent of signal intensity loss were slightly larger in the case of DS dp14 (Figure S7 of the Supporting Information).

DISCUSSION

GAGs are a frequent target of pathogens during their infection processes. An ability to inhibit pathogen−GAG interaction is therefore a promising path for therapeutic intervention. However, the many important roles GAGs play in cellular processes force any intervening therapies to target microbe−GAG interactions specifically. Detailed structural characterizations of these pathogen−GAG interactions can therefore provide valuable information about the specificities of contacts. The Borrelia protein DBPA is well-known for the crucial role it plays in the spread of Lyme disease, and results outlined in this paper will shed light on possible exploitation of its interactions with GAGs as a path to combat Lyme disease.

Because DBPA was predicted to have four helices and an attempt at high-resolution structure prediction using backbone chemical shifts and CS-ROSETTA[35] also showed the four-helix bundle as the most likely conformation, it is plausible that DBPA evolved from ancestral four-helix bundle proteins. Its present unconventional five-helix configuration may be a consequence of its function as a GAG-binding protein because this allows the crucial GAG-binding regions to form a unified binding epitope. Titration of DBPA with heparin and DS also corroborates the five-helix arrangement because this arrangement places the most perturbed residues (C-terminus and the flexible linker) in the same area around the basic pocket, whereas the four-helix bundle conformation puts them on different ends of the protein. Sequences of DBPA differ greatly among different strains of Borrelia. The structure presented in this study represents DBPA from strain B31. However, most biochemical data are obtained with strain N40 of *B. burgdorferi*. Homology models of the N40 structure constructed with the B31 structure showed that N40 DBPA preserved most of the basic residues in B31, but the BXBB motif in the flexible linker is missing. Because the results from this study indicate the linker is important in DBPA−GAG interactions, this may offer a rational explanation to the observation that N40 DBPA has a lower affinity for DS and decorin than B31 DBPA.[14]

Despite the presence of a multitude of basic amino acids throughout the protein, a well-defined, highly basic pocket does exist on DBPA. The most crucial GAG-binding residues identified by mutagenesis studies on N40 DBPA are fully preserved in the B31 version, and all three are found within the basic patch. Residues K163 and K170, together with residue R166, form a basic stretch on one face of helix 5, reminiscent of motifs commonly found in other GAG-binding helices, and the positions of the basic amino acids in the sequence (BXXBXXTB) are similar but not identical to those of consensus GAG-binding sequences identified previously.[36] Other residues forming the basic pocket include K66, K67, and K82. K136, a residue in the short linker between helices 3 and 4, is located at the periphery of the pocket and may also contribute to the basic electropotential in the region.

Ligand-induced atom chemical shift changes are often a good way of confirming the identity of the binding epitope. The heparin titration of DBPA showed the most perturbed residues are either in the C-terminus or in the linker between helices 1 and 2; both are close to the basic pocket and implicated in GAG binding.[14,17] Perturbations to many residues in the linker demonstrate that linker plays an important role in binding GAGs. Furthermore, the increases in NMR signal intensities of linker residues G69−G71 in the presence of heparin provide additional evidence of the interactions. Despite the changes heparin brought to residues in the linker, these residues were not identified as GAG binding in the peptide-based study of the interaction of strain N40 DBPA with GAGs.[17] Because the N40 version of DBPA lacks the BXBB motif, this indicates interactions of linker residues with GAGs are dependent on the BXBB motif. The K_d of DBPA's interaction with heparin dp10 is in the low millimolar range. This is in complete agreement with previous studies that showed heparin dp10 and dp12 are unable to displace *B. burgdorferi* strain N40 from Vero cells.[15] However, assuming the free energies of binding are additive when two ligands are covalently linked, the current K_d for heparin dp10 implies heparin fragments of approximately 20 monosaccharides will be sufficient to produce a low micromolar binding dissociation constant. This is also in agreement with the studies done by Leong et al.[15]

The gel mobility shift assay showed mostly monosulfated DS has a lower DBPA affinity than heparin. This offers an explanation for DS's failure to induce chemical shift changes in the titrations. However, DS fragments do interact with DBPA because their presence produced severe attenuation of signal intensities. Remarkably, residues experiencing the most signal decay are also located around the basic pocket, similar to the chemical shift perturbation patterns seen in DBPA−heparin titration. Because it has been well established that protein−ligand interactions can produce apparent increases in transverse relaxation rates of those residues perturbed by ligands, these observations provide some confirmation that these parts of DBPA may be involved in binding DS. Intriguingly, most signals appear to decay exponentially with respect to DS concentration. This cannot be easily explained by the two-state exchange theory, which stipulates that exchanges between the free and bound state of the protein lead to an apparent relaxation rate increase of $(p_1p_2) \times \Delta\omega^2/k_{ex}$, where p_1 and p_2 represent the free and bound population fractions, respectively, $\Delta\omega$ represents the change in chemical shift between free and bound states, and k_{ex} is the exchange rate constant. However, it is worth noting that when the population of ligand-bound protein is low (<10%), the increase in the transverse relaxation rate is proximately linear with respect to ligand concentration in a two-state system, which in turn leads to the exponential decay of the signal with respect to GAG concentration. If true, this argument will lead to the conclusion that short fragments of DS have a very weak affinity for DBPA. This by no means implies DS is not the target for DBPA. As for heparin, the affinities of DS fragments for a GAG-binding protein are related to their length. DS chains in vivo are often very long, with those on decorin containing ∼150 monosaccharides, which would have a much higher affinity for DBPA than fragments used in this study. It also should be noted that forms of DS purchased for this study were extracted from porcine intestinal mucosa. These have been shown to consist almost entirely of monosulfated units,[28] whereas decorin GAGs typically contain regions with higher sulfation density,[37,38] thus further boosting their affinity for DBPA. The fact that the decorin core protein is also known to play a role in its interaction with DBPA means the combined effect of DBPA−DS and DBPA−core protein interactions should make decorin DBPA's dominant binding partner in vivo.

dx.doi.org/10.1021/bi3007093 | *Biochemistry* 2012, 51, 8353−8362

Results of this study constitute a first attempt to define the GAG binding mechanism of DBPA. Effort is now underway to isolate longer fragments of heparin and DS, which may allow more well-defined structural details of the interaction to be elucidated through either traditional techniques or newer integrated approaches that have been utilized effectively in other studies.[39]

■ ASSOCIATED CONTENT

Supporting Information

Information about SDS−PAGE and SEC analysis of DBPA oligomerization, residue-specific ^{15}N rotational correlation times of DBPA, HN RDC of aligned DBPA and ^{13}C- and ^{15}N-filtered, ^{13}C-edited NOESY spectrum of DBPA, ^{15}N HSQCs of DBPA−heparin dp6 and DBPA−DS dp14 titrations, fittings of K_d for heparin−DBPA interactions, and signal intensity decay rates seen in DBPA−DS dp6 titrations. This material is available free of charge via the Internet at http://pubs.acs.org.

Accession Codes

Coordinates for the ensemble of 10 DBPA structures have been deposited in the Protein Data Bank as entry 2lqu. Atom chemical shift assignment and RDC values have been deposited in the BioMagResBank as entry 18329.

■ AUTHOR INFORMATION

Corresponding Author

*Department of Chemistry and Biochemistry, Arizona State University, Tempe, AZ 85287. E-mail: xuwang@asu.edu. Phone: (480) 727-8256.

Funding

This research was supported by a grant from the National Institute of General Medical Sciences' K99/R00 program (5R00GM088483). Grants from the National Center for Research Resources (5P41RR005351-23) and the National Institute of General Medical Sciences (8 P41 GM103390-23) from the National Institutes of Health helped to support the Resource for Integrated Glycotechnology.

Notes

The authors declare no competing financial interest.

■ ACKNOWLEDGMENTS

I thank Dr. James H. Prestegard and Dr. John Glushka of the Complex Carbohydrate Research Center for the use of their 800 MHz spectrometer and Judit Losonczi and Evgeny Tishchenko of Agilent Corp. for the use of their 800 MHz spectrometer.

■ ABBREVIATIONS

DBP, decorin-binding protein; DBPA, decorin-binding protein A; DBPB, decorin-binding protein B; GAG, glycosaminoglycan; DS, dermatan sulfate; CS, chondroitin sulfate; HSQC, heteronuclear single-quantum coherence; RDC, residual dipolar coupling; SAX, strong anion exchange; SDS-PAGE, sodium dodecyl sulfate−polyacrylamide gel electrophoresis.

■ REFERENCES

(1) Krupka, M., Zachova, K., Weigl, E., and Raska, M. (2011) Prevention of Lyme Disease: Promising Research or Sisyphean Task? *Arch. Immunol. Ther. Exp. 59*, 261−275.

(2) Fallon, B. A., Levin, E. S., Schweitzer, P. J., and Hardesty, D. (2010) Inflammation and central nervous system Lyme disease. *Neurobiol. Dis. 37*, 534−541.

(3) Halperin, J. J. (1998) Nervous system Lyme disease. *J. Neurol. Sci. 153*, 182−191.

(4) Schuijt, T. J., Hovius, J. W., van der Poll, T., van Dam, A. P., and Fikrig, E. (2011) Lyme borreliosis vaccination: The facts, the challenge, the future. *Trends Parasitol. 27*, 40−47.

(5) Guo, B. P., Brown, E. L., Dorward, D. W., Rosenberg, L. C., and Hook, M. (1998) Decorin-binding adhesins from *Borrelia burgdorferi*. *Mol. Microbiol. 30*, 711−723.

(6) Guo, B. P., Norris, S. J., Rosenberg, L. C., and Hook, M. (1995) Adherence of *Borrelia burgdorferi* to the proteoglycan decorin. *Infect. Immun. 63*, 3467−3472.

(7) Brown, E. L., Wooten, R. M., Johnson, B. J., Iozzo, R. V., Smith, A., Dolan, M. C., Guo, B. P., Weis, J. J., and Hook, M. (2001) Resistance to Lyme disease in decorin-deficient mice. *J. Clin. Invest. 107*, 845−852.

(8) Shi, Y., Xu, Q., McShan, K., and Liang, F. T. (2008) Both decorin-binding proteins A and B are critical for the overall virulence of *Borrelia burgdorferi*. *Infect. Immun. 76*, 1239−1246.

(9) Shi, Y., Xu, Q., Seemanapalli, S. V., McShan, K., and Liang, F. T. (2008) Common and unique contributions of decorin-binding proteins A and B to the overall virulence of *Borrelia burgdorferi*. *PLoS One 3*, e3340.

(10) Blevins, J. S., Hagman, K. E., and Norgard, M. V. (2008) Assessment of decorin-binding protein A to the infectivity of *Borrelia burgdorferi* in the murine models of needle and tick infection. *BMC Microbiol. 8*, 82.

(11) Weening, E. H., Parveen, N., Trzeciakowski, J. P., Leong, J. M., Hoeoek, M., and Skare, J. T. (2008) *Borrelia burgdorferi* Lacking DbpBA Exhibits an Early Survival Defect during Experimental Infection. *Infect. Immun. 76*, 5694−5705.

(12) Fischer, J. R., Parveen, N., Magoun, L., and Leong, J. M. (2003) Decorin-binding proteins A and B confer distinct mammalian cell type-specific attachment by *Borrelia burgdorferi*, the Lyme disease spirochete. *Proc. Natl. Acad. Sci. U.S.A. 100*, 7307−7312.

(13) Parveen, N., Caimano, M., Radolf, J. D., and Leong, J. M. (2003) Adaptation of the Lyme disease spirochaete to the mammalian host environment results in enhanced glycosaminoglycan and host cell binding. *Mol. Microbiol. 47*, 1433−1444.

(14) Benoit, V. M., Fischer, J. R., Lin, Y. P., Parveen, N., and Leong, J. M. (2011) Allelic variation of the Lyme disease spirochete adhesin DbpA influences spirochetal binding to decorin, dermatan sulfate, and mammalian cells. *Infect. Immun. 79*, 3501−3509.

(15) Leong, J. M., Robbins, D., Rosenfeld, L., Lahiri, B., and Parveen, N. (1998) Structural requirements for glycosaminoglycan recognition by the Lyme disease spirochete, *Borrelia burgdorferi*. *Infect. Immun. 66*, 6045−6048.

(16) Leong, J. M., Wang, H., Magoun, L., Field, J. A., Morrissey, P. E., Robbins, D., Tatro, J. B., Coburn, J., and Parveen, N. (1998) Different classes of proteoglycans contribute to the attachment of *Borrelia burgdorferi* to cultured endothelial and brain cells. *Infect. Immun. 66*, 994−999.

(17) Pikas, D. S., Brown, E. L., Gurusiddappa, S., Lee, L. Y., Xu, Y., and Hook, M. (2003) Decorin-binding sites in the adhesin DbpA from *Borrelia burgdorferi*: A synthetic peptide approach. *J. Biol. Chem. 278*, 30920−30926.

(18) Brown, E. L., Guo, B. P., O'Neal, P., and Hook, M. (1999) Adherence of *Borrelia burgdorferi*. Identification of critical lysine residues in DbpA required for decorin binding. *J. Biol. Chem. 274*, 26272−26278.

(19) Catanzariti, A. M., Soboleva, T. A., Jans, D. A., Board, P. G., and Baker, R. T. (2004) An efficient system for high-level expression and easy purification of authentic recombinant proteins. *Protein Sci. 13*, 1331−1339.

(20) Liu, Y., and Prestegard, J. H. (2009) Measurement of one and two bond N-C couplings in large proteins by TROSY-based J-modulation experiments. *J. Magn. Reson. 200*, 109−118.

(21) Liu, Y. Z., and Prestegard, J. H. (2008) Direct measurement of dipole-dipole/CSA cross-correlated relaxation by a constant-time experiment. *J. Magn. Reson. 193*, 23−31.
(22) Delaglio, F., Grzesiek, S., Vuister, G. W., Zhu, G., Pfeifer, J., and Bax, A. (1995) Nmrpipe: A Multidimensional Spectral Processing System Based on Unix Pipes. *J. Biomol. NMR 6*, 277−293.
(23) Johnson, B. A. (2004) Using NMRView to visualize and analyze the NMR spectra of macromolecules. *Methods Mol. Biol. 278*, 313−352.
(24) Cornilescu, G., Delaglio, F., and Bax, A. (1999) Protein backbone angle restraints from searching a database for chemical shift and sequence homology. *J. Biomol. NMR 13*, 289−302.
(25) Guntert, P. (2004) Automated NMR structure calculation with CYAN. *Methods Mol. Biol. 278*, 353−378.
(26) Schwieters, C. D., Kuszewski, J. J., Tjandra, N., and Clore, G. M. (2003) The Xplor-NIH NMR molecular structure determination package. *J. Magn. Reson. 160*, 65−73.
(27) Xiao, Z., Zhao, W., Yang, B., Zhang, Z., Guan, H., and Linhardt, R. J. (2011) Heparinase 1 selectivity for the 3,6-di-O-sulfo-2-deoxy-2-sulfamido-α-D-glucopyranose (1,4) 2-O-sulfo-α-L-idopyranosyluronic acid (GlcNS3S6S-IdoA2S) linkages. *Glycobiology 21*, 13−22.
(28) Yang, H. O., Gunay, N. S., Toida, T., Kuberan, B., Yu, G., Kim, Y. S., and Linhardt, R. J. (2000) Preparation and structural determination of dermatan sulfate-derived oligosaccharides. *Glycobiology 10*, 1033−1039.
(29) Seo, E. S., Blaum, B. S., Vargues, T., De Cecco, M., Deakin, J. A., Lyon, M., Barran, P. E., Campopiano, D. J., and Uhrin, D. (2010) Interaction of human β-defensin 2 (HBD2) with glycosaminoglycans. *Biochemistry 49*, 10486−10495.
(30) Lyon, M., Deakin, J. A., Lietha, D., Gherardi, E., and Gallagher, J. T. (2004) The Interactions of Hepatocyte Growth Factor/Scatter Factor and Its NK1 and NK2 Variants with Glycosaminoglycans Using a Modified Gel Mobility Shift Assay. *J. Biol. Chem. 279*, 43560−43567.
(31) Farmer, B. T., II, Constantine, K. L., Goldfarb, V., Friedrichs, M. S., Wittekind, M., Yanchunas, J., Jr., Robertson, J. G., and Mueller, L. (1996) Localizing the $NADP^+$ binding site on the MurB enzyme by NMR. *Nat. Struct. Biol. 3*, 995−997.
(32) Nabuurs, S. B., Spronk, C. A. E. M., Vuister, G. W., and Vriend, G. (2006) Traditional biomolecular structure determination by NMR spectroscopy allows for major errors. *PLoS Comput. Biol. 2*, 71−79.
(33) Holm, L., and Rosenstrom, P. (2010) Dali server: Conservation mapping in 3D. *Nucleic Acids Res. 38*, W545−W549.
(34) Parveen, N., Robbins, D., and Leong, J. M. (1999) Strain variation in glycosaminoglycan recognition influences cell-type-specific binding by lyme disease spirochetes. *Infect. Immun. 67*, 1743−1749.
(35) Shen, Y., Lange, O., Delaglio, F., Rossi, P., Aramini, J. M., Liu, G., Eletsky, A., Wu, Y., Singarapu, K. K., Lemak, A., Ignatchenko, A., Arrowsmith, C. H., Szyperski, T., Montelione, G. T., Baker, D., and Bax, A. (2008) Consistent blind protein structure generation from NMR chemical shift data. *Proc. Natl. Acad. Sci. U.S.A. 105*, 4685−4690.
(36) Hileman, R. E., Fromm, J. R., Weiler, J. M., and Linhardt, R. J. (1998) Glycosaminoglycan-protein interactions: Definition of consensus sites in glycosaminoglycan binding proteins. *BioEssays 20*, 156−167.
(37) Laremore, T. N., Ly, M., Zhang, Z., Solakyildirim, K., McCallum, S. A., Owens, R. T., and Linhardt, R. J. (2010) Domain structure elucidation of human decorin glycosaminoglycans. *Biochem. J. 431*, 199−205.
(38) Zamfir, A. D., Flangea, C., Sisu, E., Serb, A. F., Dinca, N., Bruckner, P., and Seidler, D. G. (2009) Analysis of novel over- and under-sulfated glycosaminoglycan sequences by enzyme cleavage and multiple stage MS. *Proteomics 9*, 3435−3444.
(39) Blaum, B. S., Deakin, J. A., Johansson, C. M., Herbert, A. P., Barlow, P. N., Lyon, M., and Uhrin, D. (2010) Lysine and arginine side chains in glycosaminoglycan-protein complexes investigated by NMR, cross-linking, and mass spectrometry: A case study of the factor H-heparin interaction. *J. Am. Chem. Soc. 132*, 6374−6381.